2008

The formation of polar disk galaxies

Chris B. Brook

Fabio Governato

Thomas Quinn

Beth Willman
Haverford College

The Astrophysical Journal, 689:678–686, 2008 December 20

THE FORMATION OF POLAR DISK GALAXIES

Chris B. Brook,[1] Fabio Governato,[1] Thomas Quinn,[1] James Wadsley,[2] Alyson M. Brooks,[1]
Beth Willman,[3] Adrienne Stilp,[1] and Patrik Jonsson[4]
Received 2008 February 5; accepted 2008 June 8

ABSTRACT

Polar ring galaxies, such as NGC 4650A, are a class of galaxies that have two kinematically distinct components that are inclined by almost 90° to each other. These striking galaxies challenge our understanding of how galaxies form; the origin of their distinct components has remained uncertain and is the subject of much debate. We use high-resolution cosmological simulations of galaxy formation to show that polar ring galaxies are simply an extreme example of the misalignment of angular momentum that occurs during the hierarchical structure formation characteristic of a cold dark matter cosmology. In our model, polar ring galaxies form through the continuous accretion of gas whose angular momentum is misaligned with the central galaxy.

Subject headings: cosmology: theory — galaxies: evolution — galaxies: formation

Online material: color figures, mpeg animations

1. INTRODUCTION

Significant numbers of galaxies are known to have more than one kinematically distinct component, distinguishing them as "multispin" galaxies (Rubin 1994). In some cases, these distinct kinematic structures are essentially perpendicular to each other, and such galaxies are traditionally referred to as polar ring galaxies (Whitmore et al. 1990). The formation of these exotic astronomical phenomena has been the subject of much debate (Casertano et al. 1991), and their existence has presented a logical puzzle to the way we believe that galaxies may form. Interest in polar ring galaxies is further heightened by their use in probing the nature of dark matter (Schweizer et al. 1983; Sackett et al. 1994; Iodice et al. 2006). Although it comprises 85% of the matter in the universe, we know little about the nature of dark matter. Vital clues can be found by probing its role in forming these fascinating and quixotic galaxies that have two perpendicular components.

The most extensively observed polar ring galaxies share many properties with disk galaxies, including exponential light profiles (Schweizer et al. 1983); large amounts (several times $10^9\,M_\odot$) of neutral hydrogen (H I; van Driel et al. 2000; Arnaboldi et al. 1995) in extended, rather than narrow, ring structures (van Gorkom et al. 1987; van Driel et al. 1995; Arnaboldi et al. 1997; van Driel et al. 2000; Iodice et al. 2002b; Gallagher et al. 2002); a ratio of H I mass to luminosity in the B band [$M(\mathrm{H\,I}) = L_B$] that is typical of late-type spirals (Huchtmeier 1997; Arnaboldi et al. 1997; Sparke & Cox 2000; Cox et al. 2006); young stellar populations (Gallagher et al. 2002; Karataeva et al. 2004b; Cox et al. 2006); ongoing and continuous, rather than bursty, star formation (Reshetnikov et al. 2002; Karataeva et al. 2004a); disk galaxy colors and color gradients (Reshetnikov et al. 1994; Arnaboldi et al. 1995), flat rotation curves (Reshetnikov et al. 2002; Swaters & Rubin 2003); chemical abundances typical of disk galaxies (Buttiglione et al. 2006); and spiral arms (Arnaboldi et al. 1995; Iodice et al. 2004; Cox et al. 2006). So compelling has been the evidence that links polar structures to disks in galaxies such as NGC 4650A that a change of nomenclature is occurring, with increasing reference to "polar disk galaxies" rather than "polar ring galaxies" (Iodice et al. 2006). This change in nomenclature is strongly supported by our study; for the remainder of this paper, we refer to these galaxies as polar disk galaxies.

The two scenarios for the formation of polar disk galaxies that have dominated the literature involve the interaction of two galaxies. One scenario proposes that they form in a collisional merger between two galaxies (Bekki 1998). In the second scenario, the polar disk forms from gas that is stripped from a donor galaxy that passes by the central galaxy without merging (Schweizer et al. 1983). Neither of the proposed galaxy interaction models, merger or accretion from companions, has been shown to self-consistently explain the large gas mass within the polar structure, its extended nature, and the spatial coincidence of stars with this gas (Karataeva et al. 2004b), with no evidence of interaction-induced starbursts. The merger model is also difficult to reconcile with the presence of an inner disk such as that observed, for example, in NGC 4650A (Iodice et al. 2004; disks are commonly believed to be destroyed by mergers; Barnes & Hernquist 1996). Further, both models predict that polar disk galaxies would reside preferentially in environments in which galaxy interactions are common, such as galaxy groups, yet such an environmental dependence is not observed (Brocca et al. 1997). This is emphasized by the fact that, before being reclassified as a polar ring galaxy, NGC 6822 was considered a typical isolated dwarf irregular (Demers et al. 2006). A third scenario of cold accretion claims that polar rings can be formed from the accretion of filamentary cold gas. Studies of galaxies formed in cosmological galaxy formation simulations have demonstrated that it is possible for gas accretion to be perpendicular to the central galaxy (Macciò et al. 2006, hereafter MMS06; Connors et al. 2006). In particular, MMS06 have shown that their simulated galaxy shares features with observed polar ring galaxies.

As part of a project undertaken by our group at the *N*-Body Shop that was aimed at simulating a large sample of galaxies in a cosmological context, a simulated galaxy was found (serendipitously) that had two concentric, almost perpendicular disks. This simulated galaxy, run within the "concordant" ΛCDM cosmology (Spergel et al. 2007), shares the detailed features of observed polar disk galaxies. When we compare these properties of our

[1] Department of Astronomy, University of Washington, Box 351580, Seattle, WA 98195.
[2] Department of Physics and Astronomy, McMaster University, Hamilton, ON L88 4M1, Canada.
[3] Harvard-Smithsonian Center for Astrophysics, Cambridge, MA 02138; Clay Fellow.
[4] Physics Department, University of California, Santa Cruz, CA 95064.

simulated polar disk galaxies to those observed, it is important to mimic the methods employed by observers as closely as possible. The techniques used in this study to artificially "observe" our simulated galaxy are state-of-the-art in their ability to create mock spectral energy distributions that take into account the effects of dust reprocessing. Using the age and metallicity information of the star particles in the simulations, we determine how the light of our simulated galaxy would appear when observed by the specific telescope used to observe the real galaxy to which the comparison is being made. Monte Carlo ray tracing is then used to incorporate the effects of dust reprocessing. We make particularly detailed comparisons with NGC 4650A, which is considered the prototypical polar disk galaxy (Whitmore et al. 1990).

2. METHODS

2.1. *Simulation Code*

We have used the fully parallel, *N*-body, smoothed particle hydrodynamics (SPH) code GASOLINE (Wadsley et al. 2004) to compute the evolution of the collisionless and dissipative elements. Here we outline its essential features, while the interested reader is referred to the literature for full details (Governato et al. 2007). GASOLINE computes gravitational forces using a tree code that employs multipole expansions to approximate the gravitational acceleration on each particle (Barnes & Hut 1986). Time integration is carried out using the leapfrog method, which is a second-order symplectic integrator. In cosmological simulations, it is necessary to implement periodic boundary conditions, which are achieved in GASOLINE by employing a generalized Ewald method (Hernquist et al. 1991) to fourth order.

SPH is a technique that uses particles to integrate fluid elements representing gas (Gingold & Monaghan 1977; Monaghan 1992). GASOLINE is fully Lagrangian, spatially and temporally adaptive, and efficient for large numbers of simulation particles. The code includes radiative cooling and accounts for the effect of a uniform background radiation field on the ionization and excitation state of the gas. The implemented cosmic ultraviolet background, which follows the Haardt-Madau model (Haardt & Madau 1996), includes photoionizing and photoheating rates produced by QSOs, galaxies, and Population III stars starting at $z = 10$, consistent with the combination of the third-year *WMAP* results and the Gunn-Peterson effect in the spectra of distant quasars (Alvarez et al. 2006). We use a standard cooling function for a primordial mixture of atomic hydrogen. The internal energy of the gas is integrated using the asymmetric formulation that gives results very close to those of a formalism that conserves entropy, but conserves energy better. Dissipation in shocks is modeled using the quadratic term of the Monaghan artificial viscosity (Wadsley et al. 2004), with a Balsara (Balsara 1995) correction term to reduce excessive artificial shear viscosity.

A simple but physically motivated recipe (Stinson et al. 2006) describes star formation and the effects of subsequent energy feedback from supernovae. Adopted supernova and star formation efficiency parameters were previously tested, and we use a Kroupa initial mass function (Kroupa 2001). Metal enrichment from both supernova Types Ia and II are followed on the basis of yields from the literature (Raiteri et al. 1996). The simulation described in this paper was run at the San Diego Supercomputing Facility using up to 512 CPUs, for a total of about 500,000 CPU hours.

2.2. *Cosmological Initial Conditions*

The initial conditions for the galaxy described in this paper were obtained using the so-called volume renormalization technique to achieve higher resolution in a region of interest. It is a higher resolution realization of one of the simulations already presented elsewhere (Brooks et al. 2007). The virial mass of the halo that was selected at $z = 0$ to be resimulated at higher resolution is $1.6 \times 10^{11}\ M_{\odot}$ (the virial mass is measured within the virial radius $R_{\rm vir}$, which is the radius enclosing an overdensity of 100 times the critical density $\rho_{\rm crit}$). The halo was originally selected within a low-resolution dark-matter–only simulation run in a concordance, flat, Λ-dominated cosmology: $\Omega_0 = 0.3$, $\lambda = 0.7$, $h = 70$, and $\sigma_8 = 0.9$, where Ω_0 is the matter density, Λ is the cosmological constant, h is Hubble's constant, and σ_8 is the rms fluctuation in the matter power spectrum at the 8 Mpc scale. The size of the simulated region, 28.5 Mpc, is large enough to provide realistic torques. The power spectra used to model the initial linear density field were calculated using the CMBFAST code to generate transfer functions. The dark matter, star, and gas particle masses in the high-resolution regions are 9.4×10^4, 3.3×10^3, and $1.6 \times 10^4\ M_{\odot}$, respectively. The force resolution, i.e., the gravitational softening, is 0.15 kpc. In total, there are 1.4×10^6 dark matter particles within the virial radius. At $z = 0$ there are a total of 3.5×10^6 baryonic particles within the central 20 kpc (each gas particle spawns up to three star particles and is then distributed between gas neighbors when its mass falls below 20% of what it was originally). Star particles lose mass due to supernovae and stellar winds. This mass is redistributed to nearby gas particles. With our choices of particle numbers and softening, the smallest subhalos resolved have typical circular velocities of 10% of those of their host, which ensures that all subhalos that are able to retain even a small fraction of their baryons are resolved. In subhalos with masses below $\sim 5 \times 10^9\ M_{\odot}$, the UV field prevents gas from cooling, and thus from forming stars: most subhalos with masses below this limit are empty of stars. Particles in the high-resolution region have gravitational spline softenings that were evolved in a comoving manner from the starting redshift ($z = 100$) until $z = 9$ and were then kept fixed from $z = 9$ to the present. The softening values are a compromise between reducing two-body relaxation and ensuring the spatial resolution of disk scale lengths and the central part of the dark matter halos. The simulation was run with an integration parameter of $\eta = 0.195$ and a tree code opening angle θ of 0.525 for redshifts of $z > 2$ and an opening angle of 0.725 afterward (Moore et al. 1998; Power et al. 2003). The simulated galaxy analyzed in this study is at the highest resolution of its kind in the published literature to date.

2.3. *Creation of Mock Images*

We used the open-source software Sunrise (Jonsson 2006) to generate our artificial optical images in Figures 1, 3, 6, 8, and 10. Sunrise allows us to measure the dust-reprocessed spectral energy distribution (SED) of every resolution element of our simulated galaxies from the far-UV to the far-IR with a full three-dimensional treatment of radiative transfer. Filters mimicking those on major telescopes such as the *Hubble Space Telescope* (*HST*) are used to create mock observations. Sunrise uses Monte Carlo techniques to calculate radiation transfer through astronomical dust, including such effects in the determination of SEDs.

3. EVOLUTION OF THE POLAR DISK

The scarcity of polar disk galaxies combined with the low luminosity of the polar structure makes polar disk galaxies difficult to observe at high redshift, although two candidates have been identified in the Hubble Deep Field (Reshetnikov 1997) and one in the Hubble Ultra Deep Field (Reshetnikov & Dettmar 2007). Polar disk galaxies have only been observed in detail in the nearby universe. Yet local polar disk galaxies are presently in a variety of evolutionary stages, which allows us to link properties

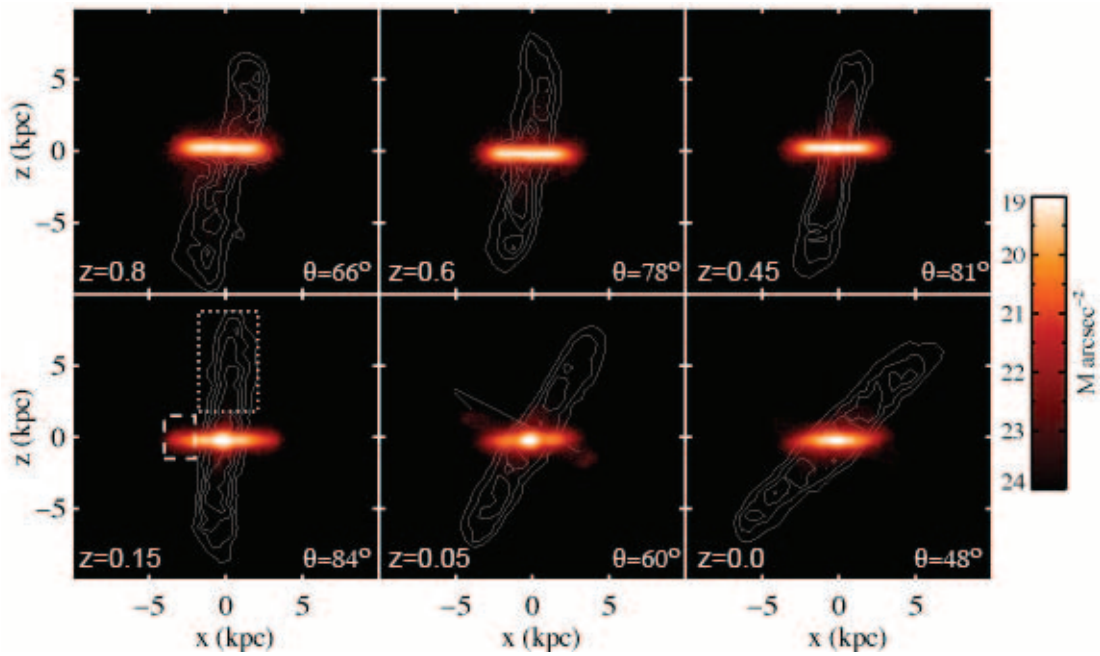

FIG. 1.—Evolution of the polar disk. At six time steps during the polar disk evolution, we make edge-on surface brightness maps of the inner disk stars, i.e., those that form between redshifts $z = 1.6$ and $z = 0.7$, in the SDSS *i*-band filter. The color bar indicates the surface brightness level in units of mag arcsec^{-2}. We overplot a contour map of the cold gas ($<4 \times 10^4$ K), where star formation takes place. At $z = 0.8$, cold gas and hence ongoing star formation are present in the inner disk, but new cold gas accretion is highly inclined to this inner disk. The angle between this new forming polar disk and the inner disk is currently 66°, as indicated in the bottom right corner of this panel. Between $z = 0.6$ and $z = 0.15$, the cold gas remains at an inclination of between 77° and 84° to the inner disk. The region indicated with the dashed box at $z = 0.15$ is selected for further analysis in Fig. 2 as being representative of the inner disk, whereas the representative polar disk stars are those within the dotted box. At $z = 0.05$, a dynamically induced morphological feature becomes apparent in the inner disk, marked as "lobes." By the present time, $z = 0$, the polar and inner disks appear to be on their way toward aligning.

of observed polar disk galaxies to different phases in the simulation and unravel a detailed history of their evolution. In the particular merging history of the simulation in which a polar disk forms, an inner disk starts forming shortly after the last major merger at redshifts of $z \sim 2$. The mass ratio of the merging galaxies is very close to 1:1, but due to its gas-rich nature, the galaxy rapidly forms a new disk whose angular momentum is largely determined by the merger orbital parameters. At later times, gas continues to be accreted to the galaxy, but in a plane that is almost perpendicular to the inner disk.

We first analyze a snapshot of the galaxy at redshift $z \sim 0.8$, shortly after the polar disk begins to form. At this time, the central galaxy is still forming stars in a disk, while the bulk of new star formation is in the highly inclined polar disk (~66° to the inner disk; see Fig. 1), with star formation continuing in both disks until $z = 0.6$ (see Fig. 2). Two prominent spiral arms are evident in the polar structure. At this stage, the galaxy shares many features of NGC 660, a local polar ring galaxy in which the central galaxy is still forming stars. The polar structure in both NGC 660 and the simulation is a disk with an exponential light profile rather than a ring, and it has a young stellar population with continuous star formation (van Driel et al. 2000). By $z = 0.5$, the inner disk has exhausted its gas, while gas continues to fall onto the polar disk. From this point in time to the present, the galaxy's star formation occurs almost exclusively in the polar disk (Fig. 2). The polar disk continues to accrete material, at an inclination that remains stable between 78 and 84° until $z = 0.15$. Almost all of the neutral hydrogen, as seen in Figure 1, is perpendicular to the inner disk during this time. The likeness to the H I maps of UGC 9796 (Cox et al. 2006) and UGC 7575 (Sparke & Cox 2000), when also overplotted on optical images that highlight their inner disk, is striking (see also § 4.3).

The polar disk in our simulation is stable for at least the 3 Gyr between $z = 0.6$ and $z = 0.15$. This is well supported by observations of stellar populations in several polar disks, which indicate that such structures are long-lived. For example, the stellar population of the polar disk in NGC 4650A has most likely been continuously forming stars for 3 Gyr (Gallagher et al. 2002; Mould et al. 1982), and the star formation observed in the polar disk of UGC 9796 indicates that it is 3–5 Gyr old (Cox et al. 2006). In the left panel of Figure 3, we make a composite image by assigning the colors blue, green, and red to mock *HST* bands

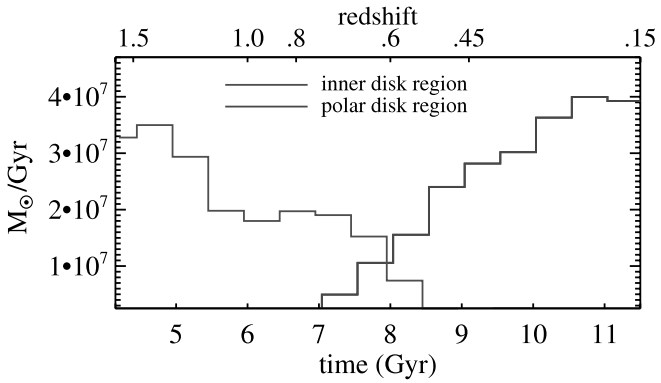

FIG. 2.—Star formation in the two disks. At $z = 0.15$, we plot the star formation history of stars within the regions corresponding to the inner (Fig. 1, *dashed box*) and polar disks (Fig. 1, *dotted box*), since the time when the inner disk begins to form. Stars form reasonably steadily within the inner disk until $z \sim 0.7$ and cease forming by $z \sim 0.5$. This reflects the lack of cold gas in the inner disk region at later times, as shown in Fig. 1. The polar disk stars began forming at $z \sim 0.7$, with relatively constant star formation for 1.5 Gyr between $z \sim 0.5$ and $z \sim 0.3$, and then constant star formation at a slightly higher rate for an additional 1.5 Gyr between $z \sim 0.3$ and $z \sim 0.15$. [*See the electronic edition of the Journal for a color version of this figure.*]

FIG. 3.—Composite image comparison with NGC 4650A. The simulated polar disk (*left*) is imaged by assigning the colors blue, green, and red to three mock *HST* bands at 450, 606, and 814 nm, respectively. The image is superimposed onto an *HST* background. NGC 4650A, which is considered to be the prototypical polar disk galaxy, is imaged (*right*) using the same assignment of image colors to *HST* bands (Gallagher et al. 2002). The red color of the inner disks reflects the old age of their stars, which emit longer wavelength light. The younger stars of the polar disks are more prominent in the shorter wavelength bands; hence their blue hue. [*This figure is a frame of an mpeg animation, available in the electronic version of the Journal, that shows the polar disk being rotated through 180°.*]

at 450, 606, and 814 nm, respectively. The image is superimposed onto an *HST* background. NGC 4650A, which is considered to be the prototypical polar disk galaxy, is imaged (*right*) using the same assignment of image colors to *HST* bands (Gallagher et al. 2002). At this time, the simulated polar disk galaxy and NGC 4650A both have extended polar disk structures with young stellar populations, ongoing star formation, blue colors, spiral arms, $M(\mathrm{H\,I})/L_B$ ratios that are typical of low surface brightness galaxies (Iodice et al. 2002b), and nearly flat rotation curves. Both have rotationally supported S0-like inner galaxies that have had little or no star formation over a period of 3 Gyr, as well as exponential light profiles (Iodice et al. 2004). Details of these properties of the inner and polar disks of the simulation are presented in § 4.

During the final 1.5 Gyr up to the present, our simulated polar disk becomes less stable, and in particular the inner regions of the polar disk begin to dynamically interact with stars in the central galaxy. This creates a complex dynamical system, with the polar and inner structures becoming less distinct. The inner regions of the polar disk galaxy ESO 603-G21 show similarly complex and overlapping dynamical structures (Reshetnikov et al. 2002). At $z \sim 0.05$, the inner disk of our simulated galaxy forms a morphological feature remarkably similar to those features described as "lobes" in the central galaxy of ESO 603-G21 (Fig. 1). These are old stars that have been dynamically stirred from the inner disk by the interaction of the two disks during this stage of the galaxy's evolution. Interestingly, ESO 603-G21 also has a polar disk that is prominent in the *K* band (Reshetnikov et al. 2002),

FIG. 4.—Snapshot from an animation of the formation of the simulated polar disk. The animation is of the same galaxy analyzed in the paper, but with 8 times fewer particles. The polar disk also forms at this resolution, which gives us confidence in our results. [*See the electronic edition of the Journal for a color version of this figure, as well as an mpeg animation.*]

indicating that, like the polar disk component of our simulation at this time, it also is several Gyr old.

3.1. *Formation Animation*

Figure 4 is a snapshot from an animation[5] showing the formation of the simulated polar disk. The animation was made "on the fly" as the simulation was being run. Unfortunately, we do not have the high-resolution run analyzed in the paper available in this format: this animation is of the same galaxy, but run with 8 times fewer particles. The formation of the polar disk remains clear at this resolution, which gives us confidence in our results. The gas in the animation is green, and the stars are white, with colored tints to indicate their age: young stars are blue, and old stars are red. The animation begins with the gas expanding with the Hubble flow, before collapsing under gravity and forming a disk. After a major merger, a disk galaxy rapidly reforms. Subsequently, gas begins to be accreted from a direction highly inclined to the inner disk. The animation ends at $z = 0.4$, at which time both an inner disk and a polar disk are evident.

4. PROPERTIES OF THE INNER AND POLAR DISKS

We refer to various properties of the two orthogonal components of our simulated polar disk galaxy in the previous section, in which we follow the galaxy's evolution. We show plots that verify these properties in this section, presented in a manner that closely mimics observations, facilitating direct comparisons with observed polar ring galaxies. In several plots, we provide distances in units of kiloparsecs, as well as arcseconds. Arcsecond scales are derived by assuming that the simulated galaxy has the same heliocentric systemic velocity as that observed for NGC 4650A (Arnaboldi et al. 1997) and using a value of 70 km s^{-1} Mpc^{-1} for the Hubble constant, which implies that $1'' = 201$ pc. Table 1 provides a summary of the properties of the simulated

[5] Available at http://www.youtube.com/watch?v=c-H3WzaewdY.

TABLE 1
GALAXY AND COMPONENT CHARACTERISTICS

Region	I_{AB}[a]	$B-I$[b]	V_{rot}[c] (km s^{-1})	V/σ_V[d]	h_l[e] (kpc)	Stellar Mass[f] ($M_\odot$)	H I Mass ($M_\odot$)	M(H I)/L_B[g] ($M_\odot/L_\odot$)
Galaxy	−20.3	1.7	...	...	...	1.0×10^{10}	2.1×10^9	0.80
Inner disk	−19.8	1.6	105	4.4	0.95	3.5×10^9	...	...
Polar disk	−19.2	1.3	115	1.4	3.4	1.6×10^9	2.1×10^9	1.4

NOTE.—Summary of the properties of the simulated galaxy, its central S0 galaxy, and the polar disk at $z = 0.15$, when the simulation most resembles NGC 4250A.
[a] The absolute magnitudes for the inner disk and the polar disk are derived by calculating the contributions to the flux from stars born before and after $z = 0.8$, after which star formation is mainly in the polar disk.
[b] The colors for the inner disk and the polar disk are for the regions indicated at $z = 0.15$ in Fig. 1.
[c] Line-of-sight velocity at 2.2 scale lengths (see Fig. 7).
[d] Measured at 2.2 scale lengths.
[e] Scale length.
[f] A significant amount of galaxy stellar mass is in an old, faint bulge/spheroid.
[g] For the region of the polar disk indicated at $z = 0.15$ in Fig. 5.

galaxy, its inner (S0 type) disk, and the polar disk at $z = 0.15$, when the simulation most resembles NGC 4250A.

4.1. *Light Profiles*

The radial surface brightness profiles of both components of our simulated polar disk galaxy attest to their disk galaxy nature. We plot these profiles in Figure 5, in two perpendicular regions as indicated in Figure 6, at $z = 0.15$. Both components have exponential light profiles outside the central bulge, with scale lengths of the inner and polar disks of approximately 0.95 and 3.4 kpc, respectively. In order to facilitate easy comparison with observations (Iodice et al. 2002a), we assume that the galaxy is at the same distance as NGC 4650A. The radius, in units of arcseconds, is indicated on the upper axis of the plot. The scale lengths of the central and polar disks of NGC 4650A are both larger than in our simulated galaxy, and both have exponential disks that ex-

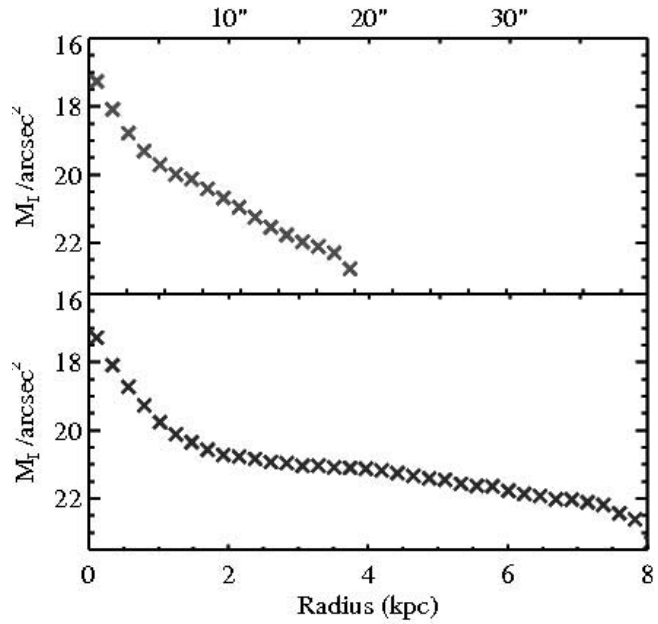

FIG. 5.—Radial surface brightness profiles in the I band, plotted for the central galaxy (*top*) and the polar disk (*bottom*). The two perpendicular regions over which the profiles are taken are indicated by the rectangles in Fig. 6. The radius is indicated in units of kiloparsecs on the lower axis of the plot. The upper axis shows the radius in units of arcseconds if the simulation were at the same distance as NGC 4650A. [*See the electronic edition of the Journal for a color version of this figure.*]

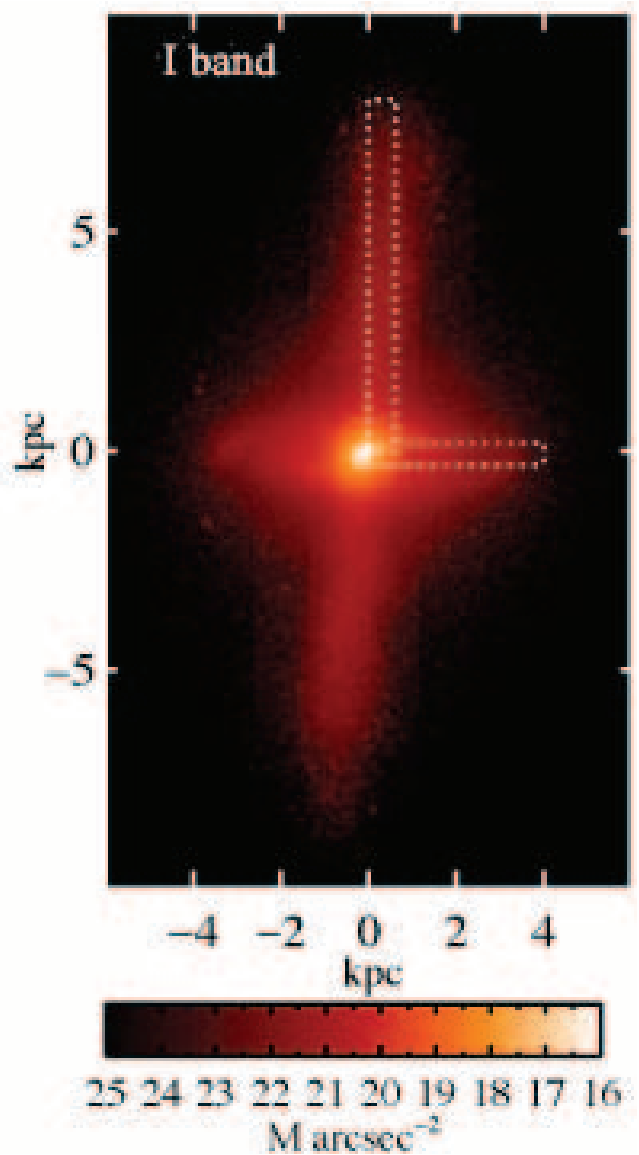

FIG. 6.—Surface brightness map in the I band. The two perpendicular regions over which the surface brightness profiles are taken in Fig. 5 are indicated by the dotted rectangles. These regions are also used for deriving the line-of-sight rotation curves in Fig. 7.

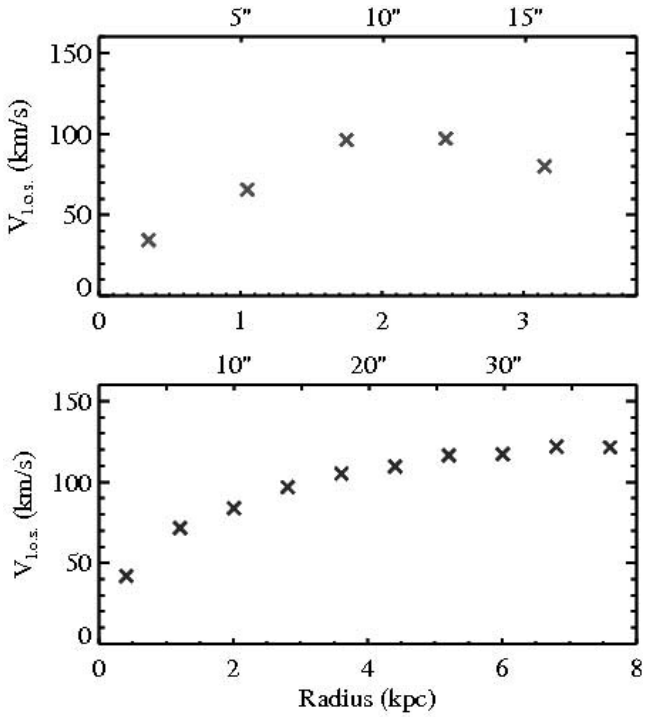

FIG. 7.—Line-of-sight velocity, vs. radius, in the two regions indicated in Fig. 6. Radial distances are provided in units of both kiloparsecs and arcseconds. The inner disk velocities (*top*) are derived using stars, while the polar disk velocities (*bottom*) were derived using cold gas ($T < 40{,}000$ K). [*See the electronic edition of the Journal for a color version of this figure.*]

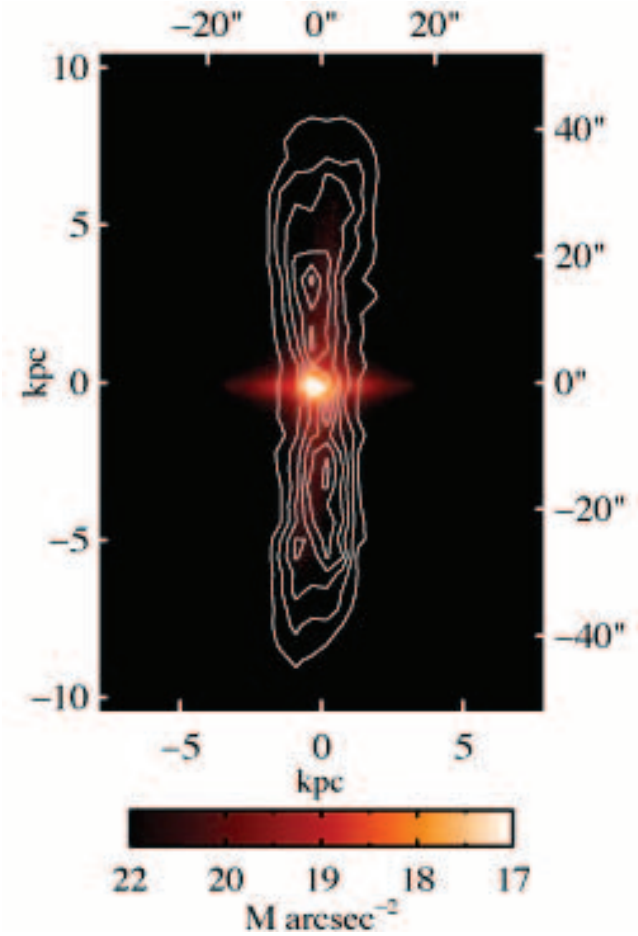

FIG. 8.—Surface brightness map of the simulation in the SDSS *r* band with the H I density map overplotted, shown at $z = 0.15$.

tend around 20% further. Yet the qualitative features are the same, and one must recall that our simulated galaxy is not a model of NGC 4650A. A high-resolution study of the light profiles of the central and polar components of a sample of five other nearby polar disk galaxies (Iodice et al. 2002b) also indicates that the presence of exponential profiles in the central galaxy is common, with all but one of the sample described as S0 systems rather than ellipticals.

4.2. *Rotation Curves*

We derive rotation curves, plotted in Figure 7, of the inner and polar disk galaxies by using the line-of-sight velocities of the stars and of the cold gas ($T < 40{,}000$ K), respectively, in the regions indicated in Figure 6. Both the inner disk and polar disk rotation curves become reasonably flat. The rotation velocity (V) at 2.2 scale lengths is very similar for both components: $\sim$105 and $\sim$115 km s^{-1} for the inner and polar disks, respectively. Radial distances are provided in units of kiloparsecs, as well as arcseconds, in order to facilitate comparison with observations (Swaters & Rubin 2003) of NGC 4650A. Both components are rotationally supported; the values of V/σ_V at 2.2 scale lengths are 1.4 and 4.4 for the inner and polar disks, respectively, where σ_V is the rotational velocity dispersion. Similar rotation curves to ours were found in the study of MMS06. The central component of NGC 4650A is also rotationally supported (Iodice et al. 2006), although the simulated central S0 galaxy is rotating significantly faster.

4.3. H I *Warps and Position-Velocity Maps*

The neutral hydrogen (H I) maps of the simulations are plotted in Figures 8 and 9. Figure 8 is an SDSS *r*-band surface brightness image, which highlights the old, central galaxy stars, with contour lines of H I gas overplotted. Almost all the H I is in the polar disk, which is virtually perpendicular to the central galaxy. The simulation is shown here at $z = 0.15$ and presents greater detail than that seen in Figure 1. The morphological features of the H I maps are very similar to those observed in polar disk galaxies such as UGC 9796 (Cox et al. 2006) and UGC 7575 (Sparke & Cox 2000). A slight integral-shaped warp is apparent in these H I maps of the simulated and observed polar disk galaxies. Such warps are evident at various times in the simulation.

The H I position-velocity map for the simulation at $z = 0.15$ is shown in Figure 9, which was computed by projecting the data onto the major axis of the polar disk. Our simulated galaxy shares the major qualitative features with the position-velocity map of NGC 4650A (Sparke & Cox 2000). In particular, both have the characteristics of a disk rather than a ring: modeling an infinitely narrow ring would produce a linear position-velocity diagram. Again, some quantitative differences with NGC 4650A are expected; in this case, the H I in the polar disk is less extended in the simulation than in the observed galaxy.

4.4. *Spiral Arms*

The polar disk of the simulated polar disk galaxy has its most prominent grand-design spiral arms at early times in its evolution. In Figure 10, we highlight the two spiral arms as they exist at $z = 0.6$ in the simulation. The surface brightness in the *V*-band image (Fig. 10*a*) is sensitive to recent star formation and shows the polar disk at an angle of 40° to edge-on, and the central galaxy's inner disk almost edge-on. The longer wavelength light imaged in the *I* band (Fig. 10*b*) is more sensitive to older stellar populations. By subtracting the *I*-band image from the *V*-band

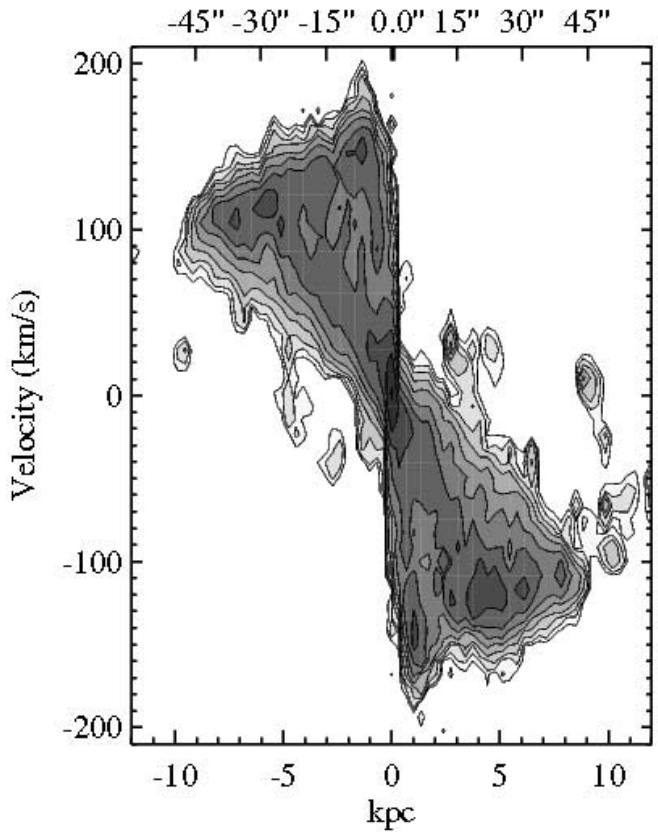

FIG. 9.—H I position-velocity map of the simulation at the same epoch as in Fig. 8. [*See the electronic edition of the Journal for a color version of this figure.*]

image, the difference, a $V - I$ image (Fig. 10*c*), highlights recent star formation, which occurs largely in the spiral arms. It is interesting that NGC 4650A also has two grand-design spiral arms (Arnaboldi et al. 1997). In our simulation, the spiral arms do not persist for the lifetime of the polar disk. The lifetime of grand-design spiral arms in numerical simulations is a complex issue, beyond the scope of this paper, but the existence of spiral arms is indicative of disklike rather than ringlike polar structures in the observed and simulated polar structures.

5. DISCUSSION

According to tidal torque theory, the misalignments of angular momentum vectors between material accreted earlier and later is expected to be common in cold dark matter structure formation, but in general the misalignment is small (Quinn & Binney 1992). Misalignment also exists between baryonic and dark matter (van den Bosch et al. 2002). In all our disk galaxy simulations, we see some misalignment of the inner disk with the later-forming outer disk at some time during its formation, resulting in a transient "integral sign" warp in the galaxy. Such warps are seen in over half of observed disk galaxies (Bosma 1991), indicating that these processes of misalignment witnessed in our simulations are real. Polar disks are the rare cases of such processes where the inclination is extreme. Such polar inclinations are seen to be stable, as is the case in our simulation.

The most stringent test of models is their ability to match a large number of observations. By significantly extending the comparison with observed polar disk galaxies, our study supports and strengthens the work of MMS06, who also found that gas flows from surrounding cosmological structures were the origin of polar disk galaxies. We have shown that such a scenario can self-consistently explain polar disk galaxy kinematics, morphologies, profiles, extended disk structures, spiral arms, colors and color gradients, longevity, and anomalous kinematic features. The uncontrived initial conditions of both MMS06 and our study are further advantages over other models for polar disk formation.

It is telling that polar disk galaxy ESO 325-G58, which is observed face-on, was classified as a barred spiral before it was shown that the "bar" was in fact an inner disk perpendicular to the line of sight (Iodice et al. 2004). Similarly, NGC 6822 is a local galaxy that was long classified as a barred irregular galaxy, but has recently been shown to be a polar ring galaxy (Demers et al. 2006). An interesting observational challenge suggested by our study is to determine the number of face-on polar disk galaxies that have been classified as barred galaxies.

This scenario may also have important implications for studying the nature of dark matter; polar disk galaxies are used as a probe of the shape of dark matter halos (Casertano et al. 1991; Schweizer et al. 1983; Sackett et al. 1994; Iodice et al. 2006). The orientation of disk galaxies with respect to their host dark halos, and with respect to the large-scale surrounding structure,

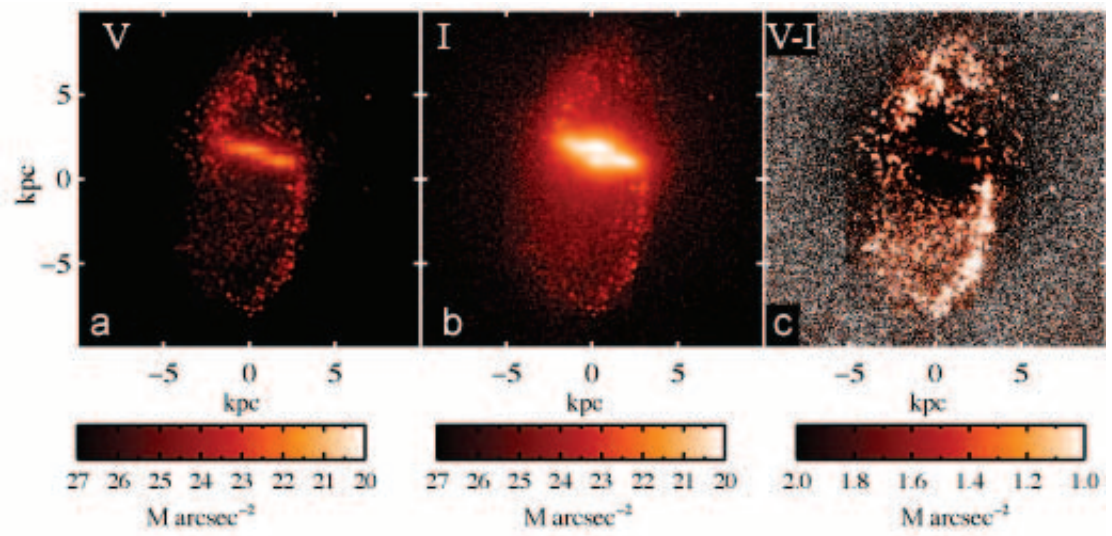

FIG. 10.—Prominence of spiral arms. (*a*) The *V*-band image is sensitive to recent star formation, and it shows the central galaxy's inner disk almost edge-on. Two prominent spiral arms are evident in the polar structure. (*b*) The longer wavelength light imaged in the *I* band is more sensitive to older stellar populations. (*c*) The $V - I$ image is derived by subtracting the *I*-band image from the *V*-band image and highlights recent star formation.

may also provide a probe of cold dark matter cosmologies. By measuring the rotation velocity in the two perpendicular disks, one can theoretically determine whether the dark matter halo is spherical, if both velocities were equal; flattened along the central galaxy, if the central disk rotates faster than the polar disk; or flattened along the polar disk, if the polar disk rotates faster than the central disk. The tendency for the inner halo alignment to be affected by the presence of the disk (Bailin et al. 2005) may have an effect on such determinations. There is also evidence that the spin axis of disk galaxies tends to be aligned with the intermediate principal axes of the local tidal tensors provided by the surrounding structure (Flin & Godlowski 1986; Navarro et al. 2004; Lee & Erdogdu 2007). Our study implies that polar disk galaxies may indeed be valuable probes of cold dark matter structure, with the ability to determine the shape of the dark matter halo being added to the potential probe of the orientation of the direction of cosmological gas flow, and how these relate to the surrounding distribution of matter in which a galaxy is embedded.

The processes of galaxy merging and accretion are both features of a cold dark matter–dominated universe, and both are capable of, indeed necessary for, producing observed properties of galaxies. The galaxies we have referred to in this study have been characterized by polar structures with disk galaxy characteristics, and we have shown that such galaxies form from cosmological gas infall. In other galaxies, such as AM 2020−504 (Whitmore et al. 1990; Arnaboldi et al. 1993), the polar structure is better described as a ring, with gas and stars in a narrow annulus. Deciding which galaxies are classified as polar rings and which as polar disks is an observational problem, which is best addressed by comparing the polar structure to the outer regions of late-type galaxies. Do polar ring and polar disk galaxies form in the same manner? There are two ways in which narrow polar structures may form within our model for polar disk galaxies. The passage of a small, satellite galaxy through a galactic disk is capable of transforming the disk into a ring. The spectacular Cartwheel galaxy is a prototype for ring galaxies (Zwicky 1941). This mechanism is capable of forming a polar ring galaxy from a polar disk galaxy (Mapelli et al. 2008). It is also possible that gas infall along a filament may have a narrow angular momentum distribution and will naturally settle into a ring. But our study is not conclusive on this issue, and the classic merging and accretion models remain viable explanations for the formation of narrow polar ring structures. For now, it may be necessary to treat polar rings and polar disks as two distinct galaxy types.

Most of the comprehensively studied polar structures are disks, and the evidence linking the polar disk structures to normal disks is compelling. The irresistible conclusion of our simulation is that the formation processes of polar disk galaxies are the same as those for the outer disk regions of normal disk galaxies, except that the polar disk forms in a different plane with respect to the central galaxy. Our scenario naturally explains the properties of several extensively studied polar disk galaxies in terms of the different stages of their evolution. The notion of "rebuilding a disk" is an essential ingredient in galaxy formation models and has been previously demonstrated in simulations (Steinmetz & Navarro 2002). Our study implies that polar disk galaxies are a spectacular demonstration of the rebuilding of disks through accretion of gas from the "cosmic web" predicted by hierarchical models of galaxy formation.

We thank Enrica Iodice for helpful discussions and Brad Gibson and Julianne Dalcanton for feedback on a draft. C. B., F. G., T. Q., and A. B. are supported by an NSF ITR grant, PHY-0205413. F. G. was supported by NSF grant AST-0607819 and by a Spitzer Theory Grant. The simulation was run at the San Diego Supercomputing Facility.

REFERENCES

Alvarez, M. A., Shapiro, P. R., Ahn, K., & Iliev, I. T. 2006, ApJ, 644, L101
Arnaboldi, M., Capaccioli, M., Barbaro, G., Buson, L., & Longo, G. 1993, A&A, 268, 103
Arnaboldi, M., Freeman, K. C., Sackett, P. D., Sparke, L. S., & Capaccioli, M. 1995, Planet. Space Sci., 43, 1377
Arnaboldi, M., Oosterloo, T., Combes, F., Freeman, K. C., & Koribalski, B. 1997, AJ, 113, 585
Bailin, J., et al. 2005, ApJ, 627, L17
Balsara, D. S. 1995, J. Comput. Phys., 121, 357
Barnes, J., & Hut, P. 1986, Nature, 324, 446
Barnes, J. E., & Hernquist, L. 1996, ApJ, 471, 115
Bekki, K. 1998, ApJ, 499, 635
Bosma, A. 1991, in Warped Disks and Inclined Rings around Galaxies, ed. S. Casertano, P. D. Sackett, & F. H. Briggs (Cambridge: Cambridge Univ. Press), 181
Brocca, C., Bettoni, D., & Galletta, G. 1997, A&A, 326, 907
Brooks, A., Governato, F., Booth, C. M., Willman, B., Gardner, J. P., Wadsley, J., Stinson, G., & Quinn, T. 2007, ApJ, 655, L17
Buttiglione, S., Arnaboldi, M., & Iodice, E. 2006, Mem. Soc. Astron. Italiana Suppl., 9, 317
Casertano, S., Sackett, P. D., & Briggs, F. H., eds. 1991, Warped Disks and Inclined Rings around Galaxies (Cambridge: Cambridge Univ. Press)
Connors, T. W., Kawata, D., Bailin, J., Tumlinson, J., & Gibson, B. K. 2006, ApJ, 646, L53
Cox, A. L., Sparke, L. S., & van Moorsel, G. 2006, AJ, 131, 828
Demers, S., Battinelli, P., & Kunkel, W. E. 2006, ApJ, 636, L85
Flin, P., & Godlowski, W. 1986, MNRAS, 222, 525
Gallagher, J. S., Sparke, L. S., Matthews, L. D., Frattare, L. M., English, J., Kinney, A. L., Iodice, E., & Arnaboldi, M. 2002, ApJ, 568, 199
Gingold, R. A., & Monaghan, J. J. 1977, MNRAS, 181, 375
Governato, F., Willman, B., Mayer, L., Brooks, A., Stinson, G., Valenzuela, O., Wadsley, J., & Quinn, T. 2007, MNRAS, 374, 1479
Haardt, F., & Madau, P. 1996, ApJ, 461, 20
Hernquist, L., Bouchet, F., & Suto, Y. 1991, ApJS, 75, 231
Huchtmeier, W. K. 1997, A&A, 319, 401
Iodice, E., Arnaboldi, M., De Lucia, G., Gallagher, J. S., III, Sparke, L. S., & Freeman, K. C. 2002a, AJ, 123, 195
Iodice, E., Arnaboldi, M., Sparke, L. S., Buta, R., Freeman, K. C., & Capaccioli, M. 2004, A&A, 418, 41
Iodice, E., Arnaboldi, M., Sparke, L. S., Gallagher, J. S., & Freeman, K. C. 2002b, A&A, 391, 103
Iodice, E., et al. 2006, ApJ, 643, 200
Jonsson, P. 2006, MNRAS, 372, 2
Karataeva, G. M., Drozdovsky, I. O., Hagen-Thorn, V. A., Yakovleva, V. A., Tikhonov, N. A., & Galazutdinova, O. A. 2004a, AJ, 127, 789
Karataeva, G. M., Tikhonov, N. A., Galazutdinova, O. A., Hagen-Thorn, V. A., & Yakovleva, V. A. 2004b, A&A, 421, 833
Kroupa, P. 2001, MNRAS, 322, 231
Lee, J., & Erdogdu, P. 2007, ApJ, 671, 1248
Macciò, A. V., Moore, B., & Stadel, J. 2006, ApJ, 636, L25 (MMS06)
Mapelli, M., Moore, B., Ripamonti, E., Mayer, L., Colpi, M., & Giordano, L. 2008, MNRAS, 383, 1223
Monaghan, J. J. 1992, ARA&A, 30, 543
Moore, B., Governato, F., Quinn, T., Stadel, J., & Lake, G. 1998, ApJ, 499, L5
Mould, J., Balick, B., Bothun, G., & Aaronson, M. 1982, ApJ, 260, L37
Navarro, J. F., Abadi, M. G., & Steinmetz, M. 2004, ApJ, 613, L41
Power, C., Navarro, J. F., Jenkins, A., Frenk, C. S., White, S. D. M., Springel, V., Stadel, J., & Quinn, T. 2003, MNRAS, 338, 14
Quinn, T., & Binney, J. 1992, MNRAS, 255, 729
Raiteri, C. M., Villata, M., & Navarro, J. F. 1996, A&A, 315, 105
Reshetnikov, V. P. 1997, A&A, 321, 749
Reshetnikov, V. P., & Dettmar, R.-J. 2007, Astron. Lett., 33, 222
Reshetnikov, V. P., Faundez-Abans, M., & de Oliviera-Abans, M. 2002, A&A, 383, 390
Reshetnikov, V. P., Hagen-Thorn, V. A., & Yakovleva, V. A. 1994, A&A, 290, 693

Rubin, V. C. 1994, AJ, 108, 456
Sackett, P. D., Rix, H., Jarvis, B. J., & Freeman, K. C. 1994, ApJ, 436, 629
Schweizer, F., Whitmore, B. C., & Ruben, V. C. 1983, AJ, 88, 909
Sparke, L. S., & Cox, A. L. 2000, in ASP Conf. Ser. 197, Dynamics of Galaxies: From the Early Universe to the Present, ed. F. Combes, G. A. Mamon, & V. Charmandaris (San Francisco: ASP), 119
Spergel, D. N., et al. 2007, ApJS, 170, 377
Steinmetz, M., & Navarro, J. F. 2002, NewA, 7, 155
Stinson, G., Seth, A., Katz, N., Wadsley, J., Governato, F., & Quinn, T. 2006, MNRAS, 373, 1074
Swaters, R. A., & Rubin, V. C. 2003, ApJ, 587, L23
van den Bosch, F. C., Abel, T., Croft, R. A. C., Hernquist, L., & White, S. D. M. 2002, ApJ, 576, 21
van Driel, W., Arnaboldi, M., Combes, F., & Sparke, L. S. 2000, A&AS, 141, 385
van Driel, W., et al. 1995, AJ, 109, 942
van Gorkom, J. H., Schechter, P. L., & Kristian, J. 1987, ApJ, 314, 457
Wadsley, J., Stadel, J., & Quinn, T. 2004, NewA, 9, 137
Whitmore, B. C., Lucas, R. A., McElroy, D. B., Steiman-Cameron, T. Y., Sackett, P. D., & Olling, R. P. 1990, AJ, 100, 1489
Zwicky, F. 1941, in Theodore von Kármán Anniversary Volume: Contributions to Applied Mechanics and Related Subjects (Pasadena: Caltech), 137